Title
Prominent Midlatitude Circulation Signature in High Asia's Surface Climate During Monsoon

Journal
Journal of Geophysical Research: Atmospheres, 122(23)

ISSN
2169-897X

Authors
Mölg, Thomas
Maussion, Fabien
Collier, Emily
et al.

Publication Date
2017-12-16

DOI
10.1002/2017jd027414

Peer reviewed

Prominent Midlatitude Circulation Signature in High Asia's Surface Climate During Monsoon

Thomas Mölg[1], Fabien Maussion[2], Emily Collier[1], John C. H. Chiang[3], and Dieter Scherer[4]

[1] Climate System Research Group, Institute of Geography, Friedrich-Alexander-University Erlangen-Nürnberg (FAU), Erlangen, Germany, [2] Institute for Atmospheric and Cryospheric Sciences, University of Innsbruck, Innsbruck, Austria, [3] Department of Geography, Center for Atmospheric Sciences, University of California, Berkeley, CA, USA, [4] Chair of Climatology, Technische Universität Berlin, Berlin, Germany

Correspondence to: T. Mölg, thomas.moelg@fau.de

Abstract

High Asia has experienced strong environmental changes in recent decades, as evident in records of glaciers, lakes, tree rings, and vegetation. The multiscale understanding of the climatic drivers, however, is still incomplete. In particular, few systematic assessments have evaluated to what degree, if at all, the midlatitude westerly circulation modifies local surface climates in the reach of the Indian Summer Monsoon. This paper shows that a southward shift of the upper-tropospheric westerlies contributes significantly to climate variability in the core monsoon season (July–September) by two prominent dipole patterns at the surface: cooling in the west of High Asia contrasts with warming in the east, while moist anomalies in the east and northwest occur with drying along the southwestern margins. Circulation anomalies help to understand the dipoles and coincide with shifts in both the westerly wave train and the South Asian High, which imprint on air mass advection and local energy budgets. The relation of the variabilities to a well-established index of midlatitude climate dynamics allows future research on climate proxies to include a fresh hypothesis for the interpretation of environmental changes.

Keywords: climate variability, High Asia, climate proxy data, circulation

1 Introduction

Climatic studies of High Asia have flourished in recent years. The drivers of this interest are the important roles of the High Asian landmass for the hemisphere-scale atmospheric circulation (Chiang et al., 2015) and the Asian water cycle (Zhang et al., 2013), together with widespread environmental changes in recent decades that illustrate strong effects of climate change in this part of the world. The observed changes concern glaciers (e.g., Bolch et al., 2012), lakes (e.g., Kropáček et al., 2012), streamflow (e.g., Zhang et al., 2013), and vegetation characteristics (e.g., Zhang et al., 2013)—phenomena that qualify as so-called climate proxies. To date, however, the climatic drivers of the observed variability and changes in proxy data are insufficiently understood, as emphasized by Bolch et al. (2012). In particular,

the link between large-scale dynamics and the local or regional surface climates deserves more attention, which would extend the room for physical interpretations of the environmental changes.

Among the existing and largely statistical efforts, relating proxy data to local meteorological time series is the dominant approach (e.g., Grießinger et al., 2016; Liang et al., 2016). A second tendency is the linkage with remote large-scale mechanisms of climate variability in the tropics (e.g., Pacific and Indian Ocean conditions) and extratropics (e.g., North Atlantic variability) (Hochreuther et al., 2016; Liang et al., 2016), which makes sense in view of High Asia's location at the interface of tropical and extratropical climates. The location aspect also matters in a third group of studies; these relate climate proxy data to the “in situ” large-scale dynamics, the extratropical westerlies and the Indian Summer Monsoon (ISM) (e.g., Benn & Owen, 1998; Li et al., 2016; Mölg et al., 2012; Yao et al., 2012). However, the said research typically regards the driver role of the two systems in separation and to be unequal. Since westerlies blow over High Asia constantly only in winter (Maussion et al., 2014), but the strongest signals in proxies all over High Asia are associated with the summer months (Grießinger et al., 2016; Liang et al., 2016; Zhu et al., 2011) during the northward progression of the monsoon, the ISM is favored in the literature for explaining climatic fluctuations at all time scales; only for individual mountain chains in northern High Asia are the westerlies deemed important (Yao et al., 2012). Yet the separation concept is not consistent with the findings from atmospheric research that the westerlies do not fully “withdraw” in summer (see below). Only a few statistical studies searched for imprints of both the westerlies and the ISM in their proxy records (Joswiak et al., 2013), and even fewer through process-based models (Mölg et al., 2014). Deepening our understanding of the combined westerlies-ISM contribution to the summertime surface-climate and environmental variability in High Asia remains an untraveled path in the recent research.

This is surprising on the one side, since atmospheric dynamics literature has long since emphasized that the interplay of both circulation systems shapes the summer climate of monsoonal Asia, starting in the 1960s (Ramaswamy, 1962) and continuing to the present (e.g., Bothe et al., 2011; Curio et al., 2015; Krishnan et al., 2009). In particular, the midlatitude westerlies over Asia are part of a circumglobal wave train in the upper troposphere (Ding & Wang, 2005), which creates linkages to the upstream climate and the North Atlantic as a consequence (Bothe et al., 2011; Liu et al., 2015; Mölg et al., 2014). Further themes of the many studies on large-scale dynamics that are relevant to the westerlies-monsoon interplay have been teleconnection routes (e.g., Bothe et al., 2011), the westerly jet stream (e.g., Schiemann et al., 2009), air-pressure patterns at the surface (e.g., Saeed et al., 2011) and in the upper troposphere (e.g., Wei et al., 2017), and the role of synoptic-scale troughs and ridges (e.g., Krishnan et al., 2009). The local patterns of

climate variability over High Asia and their specific relation to the westerly influence, however, are less well studied.

Thus, and on the other side, a quantitative framework that allows climate proxy research to consider westerly impacts in a similar fashion as ISM influences does not exist. For instance, the routine usage of an index with understandable relations to both the large-scale dynamics and regional-to-local climate variability in High Asia is not well developed for the westerlies. Hence, we postulate that valuable information about the past and recent interaction between westerlies and ISM is largely unrevealed from climate proxy archives. The goal of the present research is to attempt a step toward establishing a more systematic framework. We examine whether an index of the large-scale westerly circulation has the potential to capture significant surface-climate variability in High Asia during June–September. This goal follows the hypothesis that the activity of the midlatitude westerlies in summer appears prominently beyond the free atmosphere in the surface climate of High Asia as well. We focus on the temperature and moisture fields, which contain the variables that correlate most strongly with proxy signals (e.g., Grießinger et al., 2016; Hochreuther et al., 2016; Liang et al., 2016; Zhu et al., 2011). The findings are presented in a concise way, which intends to stimulate fresh lines of thinking in future research on proxy data from a climate dynamics angle.

2 Data and Methods

2.1 Reanalysis and Index Definitions

Reanalysis data represent a replicate of the observed atmospheric state on a global scale. The National Centers for Environmental Prediction (NCEP)/National Center for Atmospheric Research (NCAR) reanalysis (Kalnay et al., 1996) provides records since 1948, but at a rather coarse horizontal resolution of 2.5° that limits its usage for surface-climate analyses. Thus, we only consider the tropospheric levels at and above 500 hPa from this product for studying the upper half of the troposphere, which is well above the surface of High Asia (apart from localized high peaks). Humidity is only available up to 300 hPa, and thus, our wind analyses for the upper troposphere are done at this level (the results for 200 hPa winds were very similar for all analyses). The European reanalysis Era-Interim (Dee et al., 2011) is available since 1979 at a 0.75° resolution, while NASA's reanalysis MERRA, version 2 (Bosilovich et al., 2015), has a resolution of 0.5° to 0.625° (latitude and longitude, respectively) and covers 1980 onward. We include these two products in the modeling (section 2.2) and the surface-climate analyses, respectively. See Text S1 in the supporting information for data download links.

For the state of the westerlies, we follow the Global Wave Train Index (GTI) of Ding and Wang (2005). They demonstrated in detail that the GTI captures a major component of climate variability in the upper-tropospheric circulation, which is associated with the westerly jet stream. Therefore, we do not

attempt to invent a further index. The many correlations of the GTI with leading modes of climate variability over High Asia, as we will see in the results (section 3) and Table S1 in the supporting information, corroborate this choice in the given context. The GTI is simply the anomaly of the 200 hPa geopotential height, area-averaged over 35°–40°N and 60°–70°E. We multiply the GTI by −1 for easier interpretation in accordance with the theme of this study (clarified in Figure 1 caption) and will refer to as the “westerly index” hereafter. Two further indices are considered in the discussion of our results. First, the subtropical westerly jet position index defined by Zhao et al. (2014) is another one in the upper troposphere: area-averaged zonal wind at 200 hPa in a southern region (30°–45°N, 50°–80°E) minus the one in a northern region (45°–60°N, 50°–80°E). Positive deviations in the normalized time series, therefore, imply a more southerly jet position. Second is the All-India rainfall index, since it is the most widely used ISM index; its time series is readily available online (see Text S1).

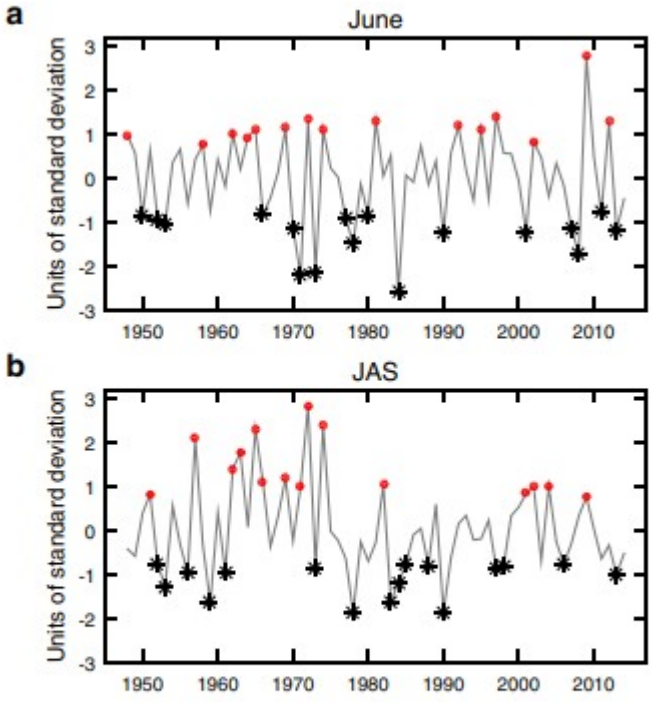

Figure 1. States of the westerly wave train. Standardized mean wave train index for (a) June and (b) July–September from 1948 to 2014. Symbols highlight distinctly positive phases (red dots; ≥0.75) and negative phases (black stars, ≤−0.75). For convenience of interpretation, the original wave train index (GTI) is multiplied by −1 in this paper, such that the positive phases coincide with W+.

Figure 1 illustrates that there were about 15 distinctly positive and negative phases of the westerly index since 1948, both in June (early monsoon season) and in the July–September (JAS) season. Positive ones coincide with an anomalously low 200 hPa surface and thus appreciable influence of the westerlies at subtropical latitudes (henceforth, W+). Negative phases indicate reduced southward influence of the west winds (W−). The difference

between contrasting composites (e.g., Ding & Wang, 2005; Saeed et al., 2011), here W+ minus W−, therefore reveals the westerly “signature” in the climatic variability. Among all the employed indices, only the GTI June time series and the ISM JAS index showed a statistically significant trend over 1948–2014 ($p < 0.05$) and were linearly detrended to focus on the interannual variability.

2.2 Atmospheric Modeling

For all years with W+ and W− cases (Figure 1) since 1980, we simulated the June–September season with version 3.8.1 of the Weather Research and Forecasting (WRF) model (Skamarock and Klemp, 2008); we used a 20 km horizontal grid spacing over a large domain that contains High Asia (Figure S1 in the supporting information) and Era-Interim as forcing data. The model settings are from a recent study and were carefully evaluated with in situ measurements from an intensive field experiment in the Himalaya (Collier & Immerzeel, 2015). Table S2 and Text S2 reveal the relevant model details.

2.3 Station Observations

We accessed all Global Historical Climatology Network station data available through the “climate explorer” platform (Table S3). The distribution of stations is sharply biased toward eastern High Asia; this feature also exists if further (nonpublically available station data) are incorporated (Liu et al., 2015). Therefore, we preferred the direct use of station data over gridded products that are based on ground observations, since the gridded fields cannot contain additional information in station-free regions. W+ and W− composites from stations typically include years before 1980 or lack some years in the 1980–2014 (MERRA and WRF) period, which demonstrates variable data availability (Table S3). However, all stations provide W+ and W− years that stretch over several decades, which should ascertain a reasonable degree of robustness in light of multidecadal patterns that are of interest here.

2.4 Statistical Applications

We employ the widely used empirical orthogonal function (EOF) analysis to extract the leading modes of atmospheric variability over High Asia, which yields the spatial patterns and the associated time series (expansion coefficient). Spatial patterns are illustrated by the so-called loadings, which measure (in dimensionless units) the strength of the relation between expansion coefficient and the local variability. Since reanalysis grid cells have different areas due to their degree resolution, we apply the cosine correction prior to the EOF to ensure that an equal area has the same contribution to the total variance of the data (Ding & Wang, 2005). We utilize North's rule of thumb to assess the uniqueness of the modes in the final EOF step (North et al., 1982).

The significance for temporal correlations is based on a two-sided t test. Those for the spatial differences in data rely on daily mean fields (to increase

the sample size and make more robust assessments) and on the Kolmogorov-Smirnov test (which can accommodate strongly skewed distributions like daily precipitation). We evaluate the *P* values from the latter test with the false discovery rate (FDR) field-significance approach of Wilks (2016). The control level is set to 0.01, so only grid cells with $p \ll 0.01$ will be significant in a spatial context (typically, an order of magnitude smaller in our case).

3 Results and Discussion

To set the context, we begin by looking at the atmospheric anomalies due to westerly influence in the upper troposphere, where the ISM-westerlies interaction originates (Bothe et al., 2011; Ding & Wang, 2005; Krishnan et al., 2009; Saeed et al., 2011). For these levels we utilize the NCEP/NCAR reanalysis product, which provides relatively long time series among available reanalyses (since 1948). Below we highlight results for the main monsoon season, JAS, but also performed all analyses for June. June conditions reflect ISM onset characteristics and may strongly impact the annual state of particular proxies (Li et al., 2016; Mölg et al., 2014), an aspect that should be considered in the discussion.

Figure 2 summarizes the patterns of the atmospheric anomalies, without addressing their significance at this stage. Strong westerlies cool the troposphere at all latitudes above West High Asia (Figure 2a) and coincide with widespread drying over classical ISM areas (Arabian Sea, India) and the southern rim regions of High Asia (Figure 2b). The associated flow anomalies reside on two action centers: an anticyclonic anomaly at higher latitudes (denoted “A” in Figure 2c) and a cyclonic anomaly at ~37°N (“B” in Figure 2c). Consequently, a strong northerly wind anomaly extends from the high latitudes to the subtropics, while the southern flank of the anomalous circulation entails enhanced westerlies at 30–35°N (Figure 2c). These meridional and zonal components favor the advection of cold and dry air typical of the westerly influence (Krishnan et al., 2009; Krishnan & Sugi, 2001; Zhao et al., 2014). A similar flow configuration was found to be important for climate variability of the Tarim Basin north of High Asia (Zhao et al., 2014). Tarim anomalies “involve matching circulation anomalies in the tropics and mid-latitudes” state Zhao et al. (2014), which underlines the result in Figure 2c that coupled anomalies across major climate zones matter. The spatially confined warm and moist anomalies in High Asia (Figures 2a and 2b) are discussed further below, as well as the aforementioned role of large-scale advection.

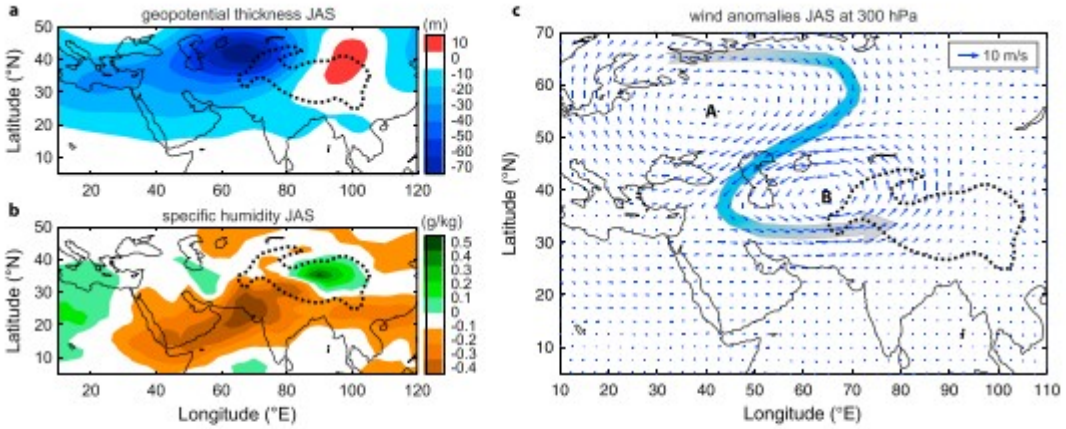

Figure 2. Effects of southward-penetrating westerlies in the upper half of the troposphere during boreal summer. Differences between W+ and W− composites in JAS, 1948–2014, for (a) geopotential thickness of the 500–200 hPa layer (reduced thickness indicates lower layer temperature), (b) vertically integrated specific humidity of the 500–300 hPa layer, and (c) wind vectors at 300 hPa, where positive zonal (westerly) and negative meridional (northerly) anomalies are indicated by the grey and blue shadings of the thick arrow, respectively, to illustrate the main pattern; the two anomaly centers connecting the system are labeled (A and B). Note that the wind arrows represent anomalies, which act upon the mean flow (Figure S2). Also note that specific humidity in NCEP/NCAR is only available up to 300 hPa, which determines the layer top for Figure 2b. The dashed line in every plot is the 2,000 m contour of terrain elevation, which roughly delineates High Asia.

However, we need to pose an essential question: are the patterns in Figure 2 significant or merely a part of random variability? The EOF analysis reveals that at least one of the two major patterns of each tropospheric temperature, humidity, and wind variability over High Asia correlates significantly (at the 1% level) with the westerly index (Table S1). Figure 3 illustrates the most relevant spatial variability patterns. W+ influence goes along with a distinct dipole pattern with cooling in the west but warming in the northeast of High Asia (Figure 3a), which closely resembles the pattern in Figure 2a. Also, the circulation anomalies of Figure 2c reappear in the leading EOF patterns of zonal and meridional winds. The zonal pattern reveals increasing westerlies during W+, except in the northwest of High Asia (Figure 3c). The meridional pattern features prominent southerly wind anomalies (orange in Figure 3d), which agree with the eastern flank of the anomaly center “B” in Figure 2c. According to the North test, these three patterns are unique since their error bars in Figure 4 (black entries) do not overlap with the adjacent modes. The situation is different for EOF2 of humidity, which correlates appreciably with the westerly index (r = 0.60) but is degenerate (Figure 4). We therefore rotated the first three EOFs of humidity with the varimax method, which is standard to extract clearer and more robust patterns (Ward, 1999). The correlation of the rotated EOF2 of humidity (REOF2) with the westerly index thereby increases, and the pattern shows that W+ promotes drying in the southwest and moistening in the northeast sector over High Asia (Figure 3b). This result aligns nicely with the interpretation from Figure 2b.

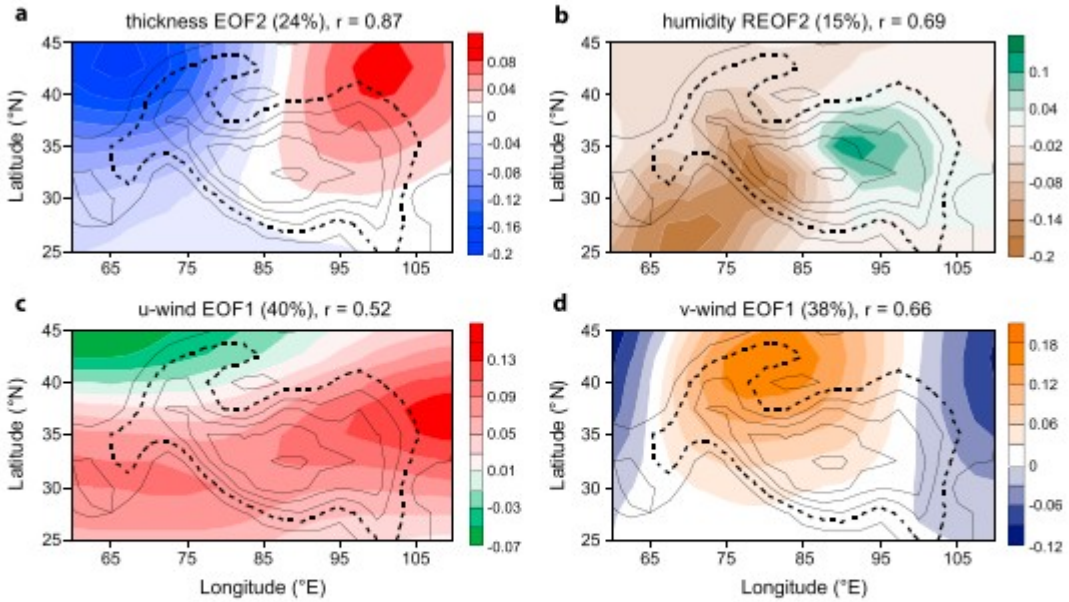

Figure 3. Leading modes of tropospheric variability over High Asia. Spatial loadings of (a) EOF2 of geopotential thickness of the 500–200 hPa layer, (b) rotated EOF2 of vertically integrated specific humidity of the 500–300 hPa layer, (c) EOF1 of zonal wind at 300 hPa, and (d) EOF1 of meridional wind at 300 hPa in JAS, 1948–2014. Explained total-field variance is given in parentheses, while *r* shows the pattern's time series correlation with the westerly index (Figure 1). The contour lines depict the topography (equidistance 1,000 m), with the 2,000 m contour emphasized.

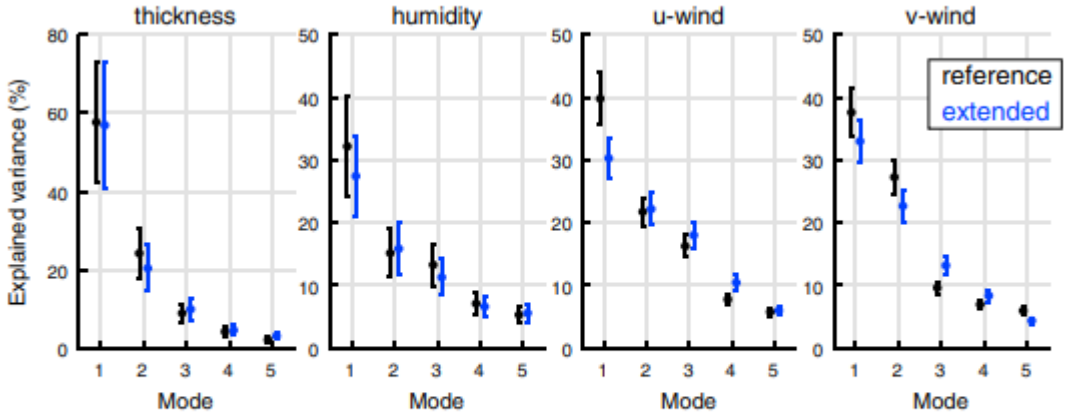

Figure 4. Robustness of the EOFs. Explained variance of the five leading EOF modes for the same variables as in Figure 3. The error bars are the result from the North et al. (1982) rule, considering autocorrelation. The black color applies to the High Asia reference domain of Figure 3 (60–100°E; 25–45°N) and the blue color to an extended domain (plus 5° at every margin).

The key features of the EOF results are not sensitive to the delineation of the High Asia domain. Taking geopotential thickness as an example, expanding the domain by 5° at every margin increases the number of grid points by 72%, yet the three leading EOF patterns remain stable. EOF2 continues to (i) explain a significant part of the total variance (20%), (ii) strongly correlate with the westerly index (r = 0.80), and (iii) be unique in North's sense; further, its spatial pattern still embodies the characteristic dipole influence

on the layer temperature evident in Figure 3a. The other EOFs of Figure 3 are similarly insensitive to the domain delineation, as illustrated in Figure 4 by the presence of the same uniqueness or degeneracy features for the modes computed using the extended domain (blue entries). The EOF analyses, therefore, corroborate that the W+-related atmospheric anomalies in Figure 2 are a significant part of the total tropospheric variability over High Asia from a statistical perspective.

The next essential question is to what extent are tropospheric anomalies manifested at the surface, where proxy phenomena are sampled? A general hurdle to answering this question is the lack of spatially complete, multidecadal surface data at an appropriate resolution (a few tens of kilometers or less); therefore, prior studies of tropospheric variability that made a link to High Asia's surface climate typically had to use data on the order of 10^2 km resolution (Bothe et al., 2011; Liu et al., 2015), which enable a basic assessment but face inherent limitations regarding spatial details (Collier & Immerzeel, 2015; Curio et al., 2015). To detect a robust W+ signature over at least the length of a climate normal period (≥30 years) and with regional to local skill, we bring together the following suite of different data (section 2): the MERRA reanalysis with a relatively high spatial resolution up to 0.5°, available meteorological station data, and results from the high-resolution atmospheric modeling forced by the Era-Interim reanalysis. The synthesis of these data in Figure 5 yields one salient feature, which is a dipole response of the surface-air temperature to W+ influence with strong cooling in the west but warming in the northeast sector of High Asia (Figures 5a and 5b). The patterns of the precipitation response are less cohesive, yet a general tendency toward wetter conditions is a robust outcome, mainly in the east and northwest of High Asia (Figures 5c and 5b). This tendency coincides with a prominent humidity increase in these regions, while reductions of air humidity only develop in the southwestern rim mountains as a part of widespread drying in Pakistan and northwest India (Figures 5e and 5f). Taken together, these results strongly suggest that (i) significant westerly related anomalies are not confined to the upper troposphere and (ii) the anomaly characteristics of the troposphere are well expressed at the surface too.

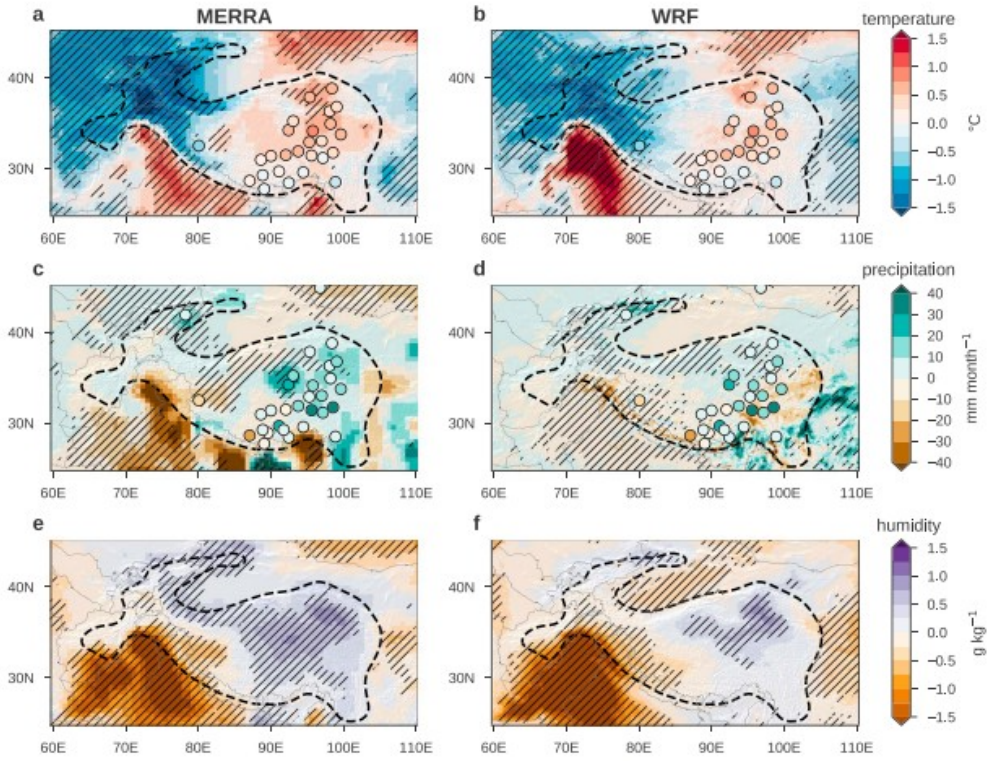

Figure 5. Effects of southward-penetrating westerlies on the surface climate in boreal summer. Differences between W+ and W− composites in JAS, 1980–2014, in the (left) MERRA and (right) WRF data sets for (a and b) 2 m air temperature, (c and d) surface precipitation, and (e and f) 2 m specific humidity. The stippled areas denote significant differences at the FDR control level of 0.01 and the dashed bold line again the 2,000 m elevation contour; the thin grey lines show national borders. Station data are included in the temperature and precipitation plots. Note that the station's W+ and W− composites may consist of sample years outside of the 1980–2014 period (see section 2.3 and Table S3).

We must finally address potential physical mechanisms that drive the tropospheric and surface response patterns described above. Cooling in the west and drying along the southwestern margin of High Asia is most certainly related to the large-scale advection properties. A cyclonic anomaly centered east of the Caspian Sea (Figure 2c) seems to be a major factor, as has been emphasized in connection with surface cooling of West Central-Asia in summer (Krishnan & Sugi, 2001). Moreover, the local surface energy budget changes (Figure S3) do not exhibit obvious west-east dipoles, which also points to the influence of large-scale advection. In this regard, the position of the upper-tropospheric westerly jet is key since the jet acts as waveguide (Ding & Wang, 2005). During W+ conditions in JAS, a southward shift of the jet is indicated by a significant correlation between the jet position index (see section 2) and the westerly index of Figure 1b ($r = 0.52$; $p < 0.01$). Figure 6 illustrates that this shift is 2°–4° on average during the summer months in the jet entrance region over High Asia, which increases the mean zonal wind south of 40°N coherently. The magnitude of the shift is significant considering the ~10° amplitude of the seasonal cycle (Schiemann et al., 2009). The importance of the jet position was also emphasized for climate variability in neighboring regions of High Asia (Zhao et al., 2014) and for East Asian monsoon seasonality (Chiang et al., 2015). Nonetheless, our

results demonstrate that jet variability cannot simply be associated with homogenous climatic anomalies over High Asia, which is a consequence of the stationary wave structure of the westerlies. In particular, tendencies for wet anomalies in the northwest and for wet/warm anomalies in regions of East High Asia appear in addition.

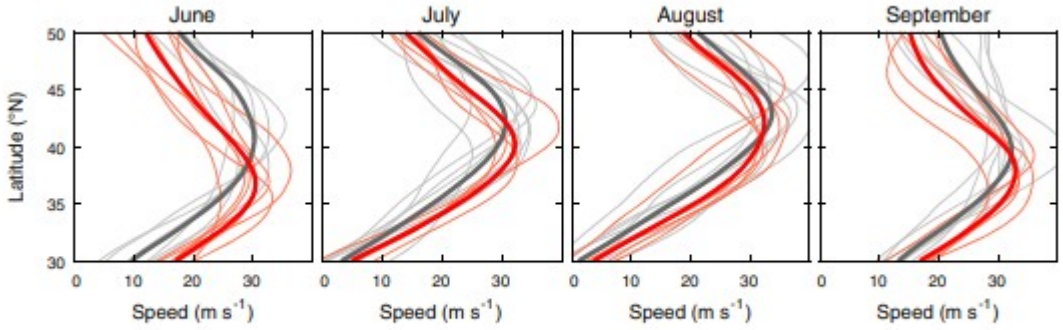

Figure 6. Jet stream shift. Monthly meridional profiles (averaged over 75°–80°E) of zonal wind velocity at 200 hPa for every month in the June–September season of a W+ year (light red) and W− year (light grey) in the 1980–2014 period (MERRA reanalysis). The thick red (dark gray) line is the mean W+ (W−) profile.

Regarding the northwest of High Asia, an obvious influence concerns reduction of the mean zonal flow in this region (Figures 3c and 6). A weaker upper-tropospheric flow is known to facilitate the development of regional convection, which is supported by observations (Mölg et al., 2009; Uyeda et al., 2001) and modeling (Collier & Immerzeel, 2015). Cold-air advection in the upper troposphere (Figure 2a) likely contributes further, since it tends to decrease the potential stability of the atmosphere. Signs of significantly enhanced convection indeed appear in the moister air over northwest High Asia: surface longwave radiation and evaporation increase, while top-of-atmosphere outgoing longwave radiation decreases (Figure S3). If we turn to the wet and warm anomalies in the eastern half (Figures 2, 3, and 5), there is one noteworthy feature. These anomalies are only observed east of the anomalous cyclonic circulation “B” (Figure 2c). Consistent local developments include enhanced heating of the atmospheric surface layer due to turbulence and longwave radiation and moistening as a result of intensified evaporation (Figure S3).

A closer look at the large-scale wave structure helps to frame the mechanisms of the varying anomaly patterns. The meridional wind in the upper troposphere demonstrates how the westerly wave stretches all from the Mediterranean Sea to North China in W+ seasons, passing over High Asia (Figure 7a). Yet in W− cases, the wave signatures end west of High Asia (Figure 7b). Figure 7c further illustrates the diminished wave activity over High Asia during weak westerlies along the 35°N latitude circle (which runs through the cooling/warming zone of West/East High Asia) and down to 500 hPa, hence near the surface of High Asia. Associated with this feature, the geopotential thickness field shows that the South Asian High retreats southward over West High Asia and advances poleward north of 30°N in East

High Asia (Figure S4); this movement is consistent with the patterns in Figures 2a and 3a. Interrelated shifts in the jet stream and the South Asian High also emerged in another recent study as drivers of opposite climate anomalies in regions of midlatitude Asia (Wei et al., 2017). Hence, contrasting temperature anomalies in High Asia during W+ despite continuous southerly flow anomalies (Figure 7c) can be explained plausibly by these shifts as well. Southerlies contribute to cooling in the west where their linkage to the strong zonal component of the anomalous cyclonic circulation “B” (Figure 2c) occurs. Yet with increasing distance from the center of “B” in the east, where the southerlies meet the expansion zone of the South Asian High, temperature advection would promote warming. Wei et al. (2017) also underline that warm-air advection from the south characterizes the eastern flank of cyclonic circulation anomalies (like “B”), which favors air ascent and precipitation. The tendency of precipitation increases in East High Asia during W+, therefore is most likely triggered by both the local moistening (Figure S3) and advective processes including water transport (e.g., Curio et al., 2015).

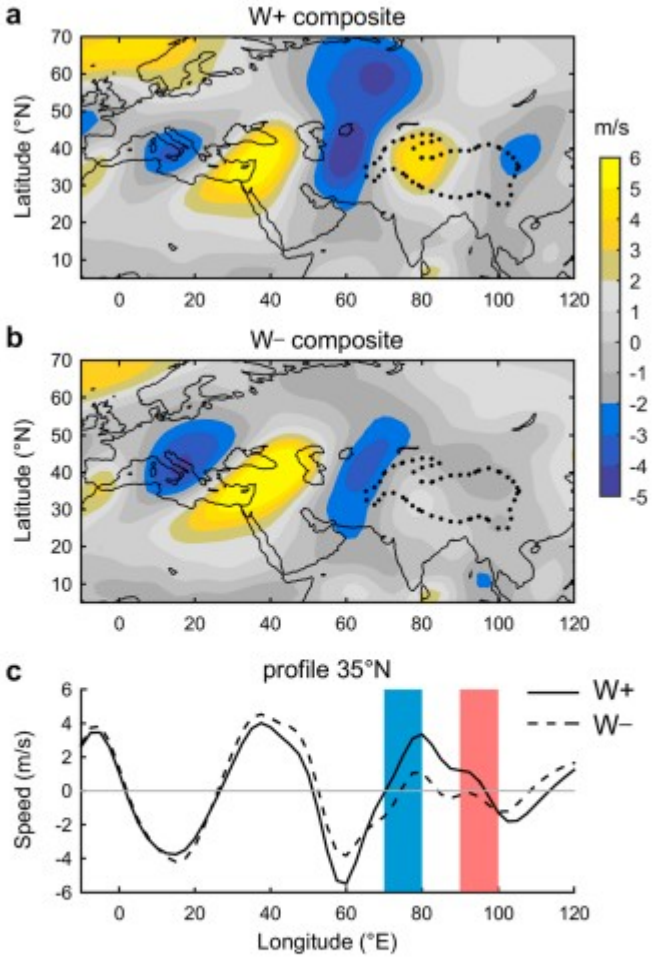

Figure 7. Tracks and strength of the westerly wave train. Mean meridional wind in JAS, 1948–2014, for (a) W+ and (b) W− phases at 300 hPa and (c) along 35°N for both phases and vertically integrated for the 500–300 hPa layer. As before, the dashed bold line in the maps is the 2,000 m elevation contour, which roughly delineates High Asia. In the bottom plot, the blue rectangle indicates the region of tropospheric and surface cooling in West High Asia during W+, while the red one signifies the region of warming in East High Asia (e.g., Figure 5, top).

The main anomaly patterns and mechanisms for JAS presented above already appear in June, except that the surface-troposphere interactions are most likely less developed (Text S3 and Figures S5 and S6). Hence, climate anomalies at the surface are less distinct in June, and capturing the potential westerly influence in the early monsoon season by proxy data may seem less obvious. However, proxies do possess this potential if the May–June season accounts for a significant fraction of their annual variability (Li et al., 2016; Mölg et al., 2014) and the underlying sensitivity shows a linkage to the upper-tropospheric climate (e.g., Mölg et al., 2014).

4 A Note on the Forcings of Westerly and ISM Influences

The results of our study could be construed as meaning the anomaly patterns in Figures 2, 3, and 5 are forced by midlatitude climate dynamics.

However, assuming that these patterns are entirely separate from the ISM state is not possible, as westerlies and ISM are interactive systems (Ding & Wang, 2005; Krishnan et al., 2009; Wei et al., 2017). A certain degree of interdependence is therefore unavoidable and manifested as statistical covariability: the westerly index and the standard ISM index (section 2.1) correlate at $r = -0.59$ (-0.63) in JAS (June) over 1948–2014 (both significant at the 1% level). This relation indicates that W+ coincides with a weak ISM. In this context, the importance of cyclonic circulation anomalies in the upper troposphere during W+ (Figure 2c) was also shown for weak ISM phases (Krishnan et al., 2009). It is none of our goals to decompose the factors of the westerlies-ISM interplay; we still provide a short synopsis of arguments below, suggesting that a southward shift of the westerlies is unlikely to be a fully passive response to ISM forcing.

(i) Ding and Wang (2005) already concluded that a clear driver role in the interaction of westerlies and ISM cannot be established and that the most promising approach is to think in terms of mutual feedbacks. Later, the results of Krishnan et al. (2009) supported this viewpoint, showing that anomalous cold-air advection by the westerlies decreases ISM convection; this reduced convection feeds back into the midlatitudes through Rossby wave dispersion, which reinforces the anomalous midlatitude circulation pattern. (ii) Some relevant mechanistic elements are clearly outside of the ISM influence. This concerns the circulation anomaly center “A” in Figure 2c, which is also evident at 850 hPa and therefore is of dynamic nature. Also, the wave activity that originates from the North Atlantic and western Europe can be considered external, since Rossby dispersion acts eastward (Ding & Wang, 2005). And (iii) correlations of the major EOF patterns of climate variability over High Asia with the ISM index are not systematically higher than the correlations with the westerly index (Table S1).

In synthesis, the surface climate anomalies during weak ISM should therefore *not* be a mirror image of Figure 5. To test this notion, we reproduced Figure 5, but this time, as the difference between weak ISM composites ($n = 10$; 1982, 1985–1987, 1991, 2000–2002, 2004, and 2009) and strong ISM composites ($n = 8$; 1983, 1988, 1990, 1994, 2005, 2006, 2007, and 2010). The +0.75 and −0.75 units of standard deviation (cf. Figure 1) again serve as the criterion for selecting strong and weak years, respectively. WRF data are not included, since the simulations were designed for westerly phases (section 2.2) and do not contain all relevant ISM years. The resulting patterns (Figure 8), however, are unmistakably robust and clearly differ from Figure 5. In particular, the westerly related dipole response in surface-air temperature does not evolve in case of the weak ISM signal (Figure 8a). Also, regions of increased precipitation in High Asia are more localized and confined to the southeast sector in the weak ISM signature (Figure 8b). Air humidity anomalies, in turn, seem to be mostly negative (Figure 8c). The greatest similarities in the response patterns of Figures 5 and 8 are outside of High Asia in the lowlands to the southwest. Although not the focus of our study,

the last point reminds us that responses to large-scale circulation variability can differ dramatically between the lowlands and the high-altitude landscapes of High Asia (e.g., Vellore et al., 2014).

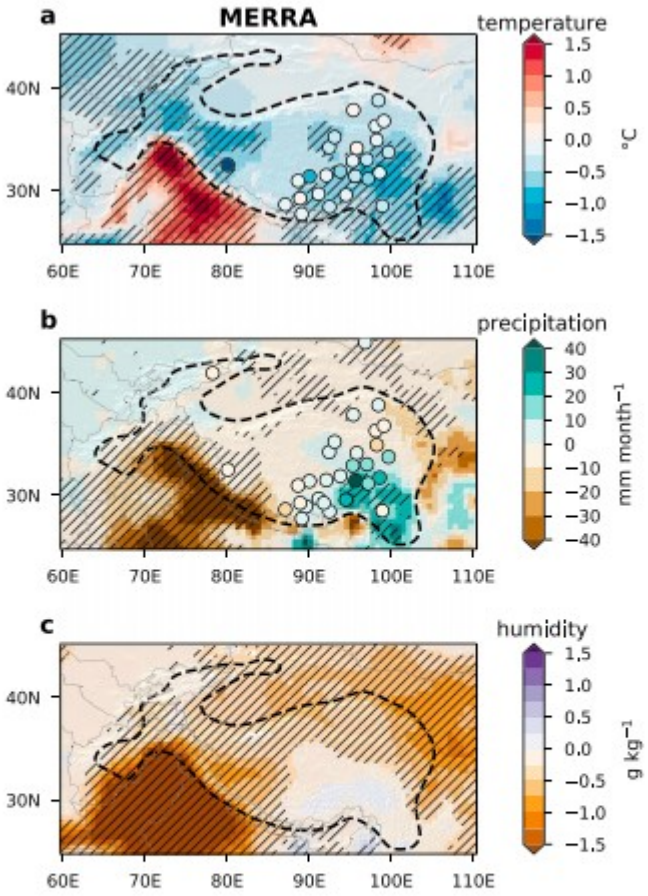

Figure 8. Effects of weak monsoon on the surface climate during boreal summer. Differences between weak ISM and strong ISM composites in JAS, 1980–2014, in the MERRA data set for (a) 2 m air temperature, (b) surface precipitation, and (c) 2 m specific humidity. The stippled areas denote significant differences at the FDR control level of 0.01 and the dashed bold line the 2,000 m elevation contour; the thin grey lines show national borders. Station data are included in the temperature and precipitation plots (as in Figure 5, the station composites may consist of sample years outside 1980–2014).

5 Concluding Remarks and Outlook

The results of our study substantiate the idea that the midlatitude westerly circulation leaves a distinct signature in the surface climate of High Asia during boreal summer. Merging three major and widely used reanalysis products, in situ observations, and atmospheric modeling increases the confidence in and robustness of the present findings. What stands out is the heterogeneous influence of strong westerly phases, in particular cold anomalies in the west and regionally confined warm/wet anomalies in the east of High Asia. It is beyond the scope of the paper to attribute the associated meridional shift of the upper-tropospheric jet to individual drivers

in the ISM-westerly interaction and its teleconnections (Ding & Wang, 2005). As discussed above, however, the westerlies most likely contribute actively to the interplay of the two circulations, which also emerges from the large-scale dynamics viewpoint (e.g., Ding & Wang, 2005; Krishnan et al., 2009).

Our study extends on previous dynamical research, by solidifying a link between the large-scale westerlies and regional-to-local climate variability in High Asia. Moreover, these results provide perspectives for future research on climate proxies. First, the demonstrated role of the westerlies creates opportunities for explaining additional variance in recent climate proxy properties; in this vein, a westerly related predictor in addition to ISM indices should also enhance the identification of atmospheric signals. Second, and regarding the paleoclimate side, reconstructed patterns of summertime moisture and temperature (e.g., Wang et al., 2016) could be used to infer past characteristics of the combined ISM-westerly influence on High Asia. This relevance exists since dominant high-frequency variability in the climate system is prone to emerge in the patterns of lower-frequency variability (Krishnan et al., 2009) or long-term changes (Vecchi and Soden, 2007) as well. The maps we present (Figure 5) and the associated inclusion of a well-founded index of the westerly waves (Ding & Wang, 2005) provide a useful basis for both avenues.

It is clear that linking our results to proxy data would be a worthwhile next step for future studies. Research along this line will also help to excite further ideas and efforts to learn about the interaction of two major circulation systems on the planet, by integrating climate dynamics knowledge and proxy data. This integration has been emphasized before as a pivotal step forward in climate research (Trenberth & Otto-Bliesner, 2003) and will benefit both disciplines.

Acknowledgments

This work was supported by the German Research Foundation (DFG) grant MO 2869/1-1 and the National Science Foundation grant AGS-1405479. We thank Yanhong Gao for the discussion on WRF data for Tibet and Kai Uwe Eiselt and Elena Kropač for assisting with the station data analysis. The WRF modeling was conducted at the High-Performance Computing Center (HPC) at the University of Erlangen-Nürnberg's Regional Computation Center (RRZE). The resultant data are only available upon request due to the very large data size. All other employed data sets are freely available (see section 2) and were obtained from the Earth System Research Laboratory (ESRL), National Aeronautics and Space Agency (NASA), European Centre for Medium-Range Forecast (ECMWF), and Dutch Meteorological Office (KNMI) platforms. The constructive comments of three anonymous reviewers improved the paper.

References

Benn, D., & Owen, L. A. (1998). The role of the Indian summer monsoon and the mid-latitude westerlies in Himalayan glaciation: Review and speculative discussion. *Journal of the Geological Society of London*, 155(2), 353– 363. https://doi.org/10.1144/gsjgs.155.2.0353

Bolch, T., Kulkarni, A., Kääb, A., Huggel, C., Paul, F., Cogley, J. G., … Stoffel, M. (2012). The state and fate of Himalayan glaciers. *Science*, 336, 310– 314. https://doi.org/10.1126/science.1215828

Bosilovich, M. G., Lucchesi, R., & Suarez, M. (2015). MERRA-2: File specification, GMAO Office Note No. 9 (Version1.0).

Bothe, O., Fraedrich, K., & Zhu, X. (2011). Large-scale circulations and Tibetan Plateau summer drought and wetness in a high-resolution climate model. *International Journal of Climatology*, 31, 832– 846. https://doi.org/10.1002/joc.2124

Chiang, J. C. H., Fung, I. Y., Wu, C. H., Cai, Y., Edman, J. P., Liu, Y., … Labrousse, C. A. (2015). Role of seasonal transitions and westerly jets in East Asian paleoclimate. *Quaternary Science Reviews*, 108, 111– 129. https://doi.org/10.1016/j.quascirev.2014.11.009

Collier, E., & Immerzeel, W. W. (2015). High-resolution modeling of atmospheric dynamics in the Nepalese Himalaya. *Journal of Geophysical Research: Atmospheres*, 120, 9882– 9896. https://doi.org/10.1002/2015JD023266

Curio, J., Maussion, F., & Scherer, D. (2015). A 12-year high-resolution climatology of atmospheric water transport over the Tibetan Plateau. *Earth System Dynamics*, 6(1), 109– 124. https://doi.org/10.5194/esd-6-109-2015

Dee, D. P., Uppala, S. M., Simmons, A. J., Berrisford, P., Poli, P., Kobayashi, S., … Vitart, F. (2011). The ERA-Interim reanalysis: Configuration and performance of the data assimilation system. *Quarterly Journal of the Royal Meteorological Society*, 137, 553– 597. https://doi.org/10.1002/qj.828

Ding, Q., & Wang, B. (2005). Circumglobal teleconnection in the Northern Hemisphere summer. *Journal of Climate*, 18(17), 3483– 3505. https://doi.org/10.1175/JCLI3473.1

Grießinger, J., Bräuning, A., Helle, G., Hochreuther, P., & Schleser, G. (2016). Late Holocene relative humidity history on the southeastern Tibetan Plateau inferred from a tree-ring $\delta^{18}O$ record: Recent decrease and conditions during the last 1500 years. *Quaternary International*, 430, 52– 59. https://doi.org/10.1016/j.quaint.2016.02.011

Hochreuther, P., Wernicke, J., Grießinger, J., Mölg, T., Zhu, H., Liang, E., … Bräuning, A. (2016). Influence of the Indian Ocean Dipole on tree-ring δ18O of monsoonal southeast Tibet. *Climatic Change*, 137(1-2), 217– 230. https://doi.org/10.1007/s10584-016-1663-8

Joswiak, D. R., Yao, T., Wu, G., Tian, L., & Xu, B. (2013). Ice-core evidence of westerly and monsoon moisture contributions in the central Tibetan Plateau. *Journal of Glaciology*, 59(213), 56– 66. https://doi.org/10.3189/2013JoG12J035

Kalnay, E., Kanamitsu, M., Kistler, R., Collins, W., Deaven, D., Gandin, L., … Joseph, D. (1996). The NCEP/NCAR 40-year reanalysis project. *Bulletin of the American Meteorological Society*, 77(3), 437– 471. https://doi.org/10.1175/1520-0477(1996)077%3C0437:TNYRP%3E2.0.CO;2

Krishnan, R., Kumar, V., Sugi, M., & Yoshimura, J. (2009). Internal feedbacks from monsoon-midlatitude interactions during droughts in the Indian summer monsoon. *Journal of the Atmospheric Sciences*, 66, 553– 578. https://doi.org/10.1175/2008JAS2723.1

Krishnan, R., & Sugi, M. (2001). Baiu rainfall variability and associated monsoon teleconnections. *Journal of the Meteorological Society of Japan*, 79(3), 851– 860. https://doi.org/10.2151/jmsj.79.851

Kropáček, J., Braun, A., Kang, S., Feng, C., Ye, Q., & Hochschild, V. (2012). Analysis of lake level changes in Nam Co in central Tibet utilizing synergistic satellite altimetry and optical imagery. *International Journal of Applied Earth Observation*, 17, 3– 11. https://doi.org/10.1016/j.jag.2011.10.001

Li, R., Luo, T., Mölg, T., Zhao, J., Li, X., Cui, X., … Tang, Y. (2016). Leaf unfolding of Tibetan alpine meadows captures the arrival of monsoon rainfall. *Scientific Reports*, 6(1), 20,985. https://doi.org/10.1038/srep20985

Liang, H., Lyu, L., & Wahab, M. (2016). A 382-year reconstruction of August mean minimum temperature from tree-ring maximum latewood density on the southeastern Tibetan Plateau, China. *Dendrochronologia*, 37, 1– 8. https://doi.org/10.1016/j.dendro.2015.11.001

Liu, H., Duan, K., Li, M., Shi, P., Yang, J., Zhang, X., & Sun, J. (2015). Impact of the North Atlantic Oscillation on the dipole oscillation of summer precipitation over the central and eastern Tibetan Plateau. *International Journal of Climatology*, 35(15), 4539– 4546. https://doi.org/10.1002/joc.4304

Maussion, F., Scherer, D., Mölg, T., Collier, E., Curio, J., & Finkelnburg, R. (2014). Precipitation seasonality and variability over the Tibetan Plateau as resolved by the High Asia reanalysis. *Journal of Climate*, 27(5), 1910– 1927. https://doi.org/10.1175/JCLI-D-13-00282.1

Mölg, T., Chiang, J. C. H., Gohm, A., & Cullen, N. J. (2009). Temporal precipitation variability versus altitude on a tropical high mountain: Observations and mesoscale atmospheric modeling. *Quarterly Journal of the Royal Meteorological Society*, 135, 1439– 1455. https://doi.org/10.1002/qj.461

Mölg, T., Maussion, F., & Scherer, D. (2014). Mid-latitude westerlies as a driver of glacier variability in monsoonal High Asia. *Nature Climate Change*, 4(1), 68– 73. https://doi.org/10.1038/NCLIMATE2055

Mölg, T., Maussion, F., Yang, W., & Scherer, D. (2012). The footprint of Asian monsoon dynamics in the mass and energy balance of a Tibetan glacier. *The Cryosphere*, 6, 1445– 1461. https://doi.org/10.5194/tc-6-1445-2012

North, G. R., Bell, T. L., Cahalan, R. F., & Moeng, F. J. (1982). Sampling errors in the estimation of empirical orthogonal functions. *Monthly Weather Review*, 110(7), 699– 706. https://doi.org/10.1175/1520-0493(1982)110%3C0699:SEITEO%3E2.0.CO;2

Ramaswamy, C. (1962). Breaks in the Indian summer monsoon as a phenomenon of interaction between the easterly and the sub-tropical westerly jet streams. *Tellus*, 14(3), 337– 349.

Saeed, S., Müller, W. A., Hagemann, S., & Jacob, D. (2011). Circumglobal wave train and the summer monsoon over northwestern India and Pakistan: The explicit role of the surface heat low. *Climate Dynamics*, 37, 1045– 1060. https://doi.org/10.1007/s00382-010-0888-x

Schiemann, R., Lüthi, D., & Schär, C. (2009). Seasonality and interannual variability of the westerly jet in the Tibetan Plateau region. *Journal of Climate*, 22(11), 2940– 2957. https://doi.org/10.1175/2008JCLI2625.1

Skamarock, W. C., & Klemp, J. B. (2008). A time-2split nonhydrostatic atmospheric model for weather research and forecasting applications. *Journal of Computational Physics*, 227(7), 3465– 3485. https://doi.org/10.1016/j.jcp.2007.01.037

Trenberth, K. E., & Otto-Bliesner, B. L. (2003). Toward integrated reconstruction of past climates. *Science*, 300(5619), 589– 590. https://doi.org/10.1126/science.1083122

Uyeda, H., Yamada, H., Horikomi, J., Shirooka, R., Shimizu, S., Liping, L., … Koike, T. (2001). Characteristics of convective clouds observed by a Doppler radar at Naqu on Tibetan Plateau during the GAME-Tibet IOP. *Journal of the Meteorological Society of Japan*, 79(1B), 463– 474. https://doi.org/10.2151/jmsj.79.463

Vecchi, G. A., & Soden, B. J. (2007). Global warming and the weakening of the tropical circulation. *Journal of Climate*, 20(17), 4316– 4340. https://doi.org/10.1175/JCLI4258.1

Vellore, R. K., Krishnan, R., Pendharkar, J., Choudhury, A. D., & Sabin, T. P. (2014). On the anomalous precipitation enhancement over the Himalayan foothills during monsoon breaks. *Climate Dynamics*, 43(7-8), 2009– 2031. https://doi.org/10.1007/s00382-013-2024-1

Wang, M., Liang, J., Hou, J., & Hu, L. (2016). Distribution of GDGTs in lake surface sediments on the Tibetan Plateau and its influencing factors. *Science China Earth Sciences*, 59(5), 961– 974. https://doi.org/10.1007/s11430-015-5214-3

Ward, M. N. (1999). Analyzing the boreal summer relationship between worldwide sea-surface temperature and atmospheric variability. In H. Von Storch & A. Navarra (Eds.), *Analysis of Climate Variability* (pp. 95– 118). Berlin, Heidelberg and New York: Springer. https://doi.org/10.1007/978-3-662-03744-7_6

Wei, W., Zhang, R., Wen, M., & Yang, S. (2017). Relationship between the Asian westerly jet stream and summer rainfall over Central Asia and North China: Roles of the Indian monsoon and the South Asian High. *Journal of Climate*, 30(2), 537– 552. https://doi.org/10.1175/JCLI-D-15-0814.1

Wilks, D. S. (2016). “The stippling shows statistically significant grid points”. How research results are routinely overstated and overinterpreted, and what to do about it. *Bulletin of the American Meteorological Society*, 97(12), 2263– 2273. https://doi.org/10.1175/BAMS-D-15-00267.1

Yao, T., Thompson, L. G., Yang, W., Yu, W., Gao, Y., Guo, X., … Joswiak, D. (2012). Different glacier status with atmospheric circulations in Tibetan Plateau and surroundings. *Nature Climate Change*, 2, 663– 667. https://doi.org/10.1038/NCLIMATE1580

Zhang, L., Su, F., Yang, D., Hao, Z., & Tong, K. (2013). Discharge regime and simulation for the upstream of major rivers over Tibetan Plateau. *Journal of Geophysical Research: Atmospheres*, 118, 8500– 8518. https://doi.org/10.1002/jgrd.50665

Zhang, Y., Zhang, J., & Dong, X. X. (2013). Green-up dates in the Tibetan Plateau have continuously advanced from 1982 to 2011. *Proceedings of the National Academy of Sciences of the United States of America*, 110(11), 4309– 4314. https://doi.org/10.1073/pnas.1210423110

Zhao, Y., Huang, A., Zhou, Y., Huang, D., Yang, Q., Ma, Y., … Wei, G. (2014). Impact of the middle and upper tropospheric cooling over central Asia on the summer rainfall in the Tarim Basin, China. *Journal of Climate*, 27(12), 4721– 4732. https://doi.org/10.1175/JCLI-D-13-00456.1

Zhu, H. F., Shao, X. M., Yin, Z. Y., Xu, P., Xu, Y., & Tian, H. (2011). August temperature variability in the southeastern Tibetan Plateau since AD 1385 inferred from tree rings. *Palaeogeography Palaeoclimatology Palaeoecology*, 305, 84– 92. https://doi.org/10.1016/j.palaeo.2011.02.017